J|A|C|S
ARTICLES
Published on Web 02/10/2007

Reactive Nature of Dopamine as a Surface Functionalization Agent in Iron Oxide Nanoparticles

Michael D. Shultz,[†] J. Ulises Reveles,[‡] Shiv N. Khanna,[‡] and Everett E. Carpenter*,[†]

Contribution from the Departments of Chemistry and Physics, Virginia Commonwealth University, Richmond, Virginia 23284

Received July 31, 2006; E-mail: ecarpenter2@vcu.edu

Abstract: Dopamine forms an initial structure coordinated to the surface of the iron oxide nanoparticle as a result of improved orbital overlap of the five-membered ring and a reduced steric environment of the iron complex. However, through transfer of electrons to the iron cations on the surface and rearrangement of the oxidized dopamine, a semiquinone is formed. Because of free protons in the system, oxygens on the surface are protonated, which allows for the Fe^{2+} to be released into the solution as a hydroxide. This released fragment of the nanoparticle will then eventually oxidize in air to a form of an iron(III) oxyhydroxide. All of the reported results demonstrate that the reactivity between Fe^{3+} and dopamine quickly facilitates the degradation of the nanoparticles. The energetic modeling studies substantiate our proposed decomposition mechanism and thus conclude that the use of dopamine as a robust anchor for iron oxide or iron oxide shell particles will not fulfill the need for stable ferrofluids in most biomedical applications.

1. Introduction

Magnetic nanoparticles based on iron oxides or iron oxide shells are flourishing in biotechnology and medical applications. These applications include use as magnetic resonance imaging (MRI) contrast agents,[1−3] ferrofluid technology for MRI monitoring in hypothermia,[4,5] cancer tumor detection via SQUID magnetometry,[6] and selective separation and detection of biomolecules.[7,8] The appeal of these particles is due to their relative inertness, superior magnetic properties, and the apparent simplicity of postsynthesis surface functionalization.

Stability of the bonding between functional molecules and nanoparticles is crucial for most medical applications because the particle is the key to tracking or targeting treatments that the functional molecule is to perform. Early release or uptake of the nanoparticle/molecule system due to other surface reactions could be detrimental to the application or possibly to the patient. While carboxylic acids have been used as stabilizers for ferrofluid applications, they typically are not an ideal functionalization ligand due to the instability of the chelate bond. It has been reported that dopamine forms a stable, robust anchor on the surface of iron oxide to immobilize functional molecules to the magnetic nanoparticles.[9] Dopamine has sparked great interest as capping agent due to the stability and strength of the resultant five-membered metallocycle chelate and the ease at which it can be functionalized through amide bonds with other molecules of interest.

This study reports on the structure and reactivity of Fe/iron oxide core−shell nanoparticles (Fe−Ox) that have been coated with dopamine. Through experimental and theoretical methods, we show that a surface reaction occurs between dopamine and Fe^{3+} and discuss the mechanism that leads to the nanoparticles precipitating out of solution. We also confirm the presence of the dopamine quinone, which is highly reactive and is suggested to be cytotoxic.[10]

2. Experimental Section

2.1. Materials and Instrumentation. Iron(II) chloride tetrahydrate, nickel(II) chloride hexahydrate, and sodium borohydride were all purchased from ACROS Organics. Cyclohexane, chloroform, and methanol were purchased from Fisher Scientific. Surfactants used were nonylphenoxy poly(ethyleneoxy)ethanols known by product names IGEPAL CO-430 (NP4) for a chain length of five and IGEPAL CO-610 (NP7) for a chain length of nine and were received from Rhodia Inc. Diacid polyethylene glycol (PEG, MW: 600 g/mol) was purchased from Fluka, and dopamine hydrochloride was purchased from Alfa Aesar. The orthoquinone used was 3,5-di-*tert*-butyl-1,2-benzoquinone and was purchased from Aldrich. All chemicals were used as received without further purification.

[†] Department of Chemistry.
[‡] Department of Physics.

(1) Kohler, N.; Fryxell, G. E.; Zhang, M. *J. Am. Chem. Soc.* **2004**, *126*, 7206.
(2) Jun, Y.-w.; Huh, Y.-M.; Choi, J.-s.; Lee, J.-H.; Song, H.-T.; Kim, S.; Yoon, S.; Kim, K.-S.; Shin, J.-S.; Suh, J.-S.; Cheon, J. *J. Am. Chem. Soc.* **2005**, *127*, 5732.
(3) Veiseh, O.; Sun, C.; Gunn, J.; Kohler, N.; Gabikian, P.; Lee, D.; Bhattarai, N.; Ellenbogen, R.; Sze, R.; Hallahan, A.; Olson, J.; Zhang, M. Q. *Nano Lett.* **2005**, *5*, 1003.
(4) Reinl, H. M.; Peller, M.; Hagmann, M.; Turner, P.; Issels, R. D.; Reiser, M. *Magn. Reson. Imaging* **2005**, *23*, 1017.
(5) Hergt, R.; Hiergeist, R.; Hilger, I.; Kaiser, W. A.; Lapatnikov, Y.; Margel, S.; Richter, U. *J. Magn. Magn. Mater.* **2004**, *270*, 345.
(6) Kenning, G. G.; Rodriguez, R.; Zotev, V. S.; Moslemi, A.; Wilson, S.; Hawel, L.; Byus, C.; Kovach, J. S. *Rev. Sci. Instrum.* **2005**, *76*, 014303−1.
(7) Perez, J. M.; Simeone, F. J.; Saeki, Y.; Josephson, L.; Weissleder, R. *J. Am. Chem. Soc.* **2003**, *125*, 10192.
(8) Wang, D.; He, J.; Rosenzweig, N.; Rosenzweig, Z. *Nano Lett.* **2004**, *4*, 409.
(9) Xu, C. J.; Xu, K. M.; Gu, H. W.; Zheng, R. K.; Liu, H.; Zhang, X. X.; Guo, Z. H.; Xu, B. *J. Am. Chem. Soc.* **2004**, *126*, 9938.
(10) Clarke, S. J.; Hollmann, C. A.; Zhang, Z.; Suffern, D.; Bradforth, S. E.; Dimitrijevic, N.; Minarik, W. G.; Nadeau, J. L. *Nat. Mater.* **2006**, *5*, 409.

10.1021/ja0651963 CCC: $37.00

Samples were prepared for FT-IR by grinding them with mortar and pestle into a mixture with silver bromide (AgBr) at approximately a 1:10 mass ratio. The mixture was then pressed in a 13 mm pellet die at an applied load of 9 tons, to yield approximately 1 mm thick pellets. The spectra were collected on a Nicolet Nexus 670 FT-IR with a KBr beam splitter, deuterated triglycine sulfate (DTGS) detector, and a purge cell apparatus to minimize moisture in the measuring environment. A single beam background spectrum was taken to minimize CO_2 and H_2O signals in the measurements. A AgBr spectrum was collected and used for the background subtraction of each sample. AgBr was used for far-IR and for the mid-IR when looking only at the OH stretch region because AgBr should allow for easier handling and less water interference. Other mid-IR ranges were taken on samples prepared in KBr pellets. UV−vis absorption analysis was carried out using a Hewlett-Packard 8452A diode array spectrophotometer, and all solutions were aqueous except the orthobenzoquinone, which was prepared in cyclohexane. Transmission electron micrographs were taken on a Jeol JEM-1230 at 120 kV with a Gatan Ultra Scan 4000 SP 4Kx4K CCD camera, and slides were prepared on Formvar/carbon 200 mesh copper grids. Magnetic characterization was conducted on a Quantum Design superconducting quantum interference device (SQUID). Elemental analysis by inductively coupled plasma-optical emission spectroscopy (ICP) was performed using a Varian Vista-MPX ICP-OES. Samples were prepared for ICP by dissolving them with 2 mL of concentrated nitric acid. To ensure complete dissociation of all components, the solution was placed in a 23 mL Parr Instrument Co. acid digestion bomb (model 4749 with PTFE cup insert) overnight at 160 °C and then diluted to 100 mL.

2.2. Synthesis. The synthesis of core−shell nanoparticles was carried out using Schlenk line techniques and the reverse micelle method.[11] First, 80 mL of C_6H_{12}, 13.7 mL of NP4, and 20.6 mL of NP7 were mixed in a round-bottom flask and degassed under nitrogen for 20 min. A second solution was prepared combining half of each of the above quantities and subsequent addition of 4.633 mL of a 0.518 M Ni^{2+}(aq). This solution was stirred by vortex until clear (micelle formation), placed in an addition funnel, and degassed. Next, 6.83 mL of a 0.70 M Fe^{2+}(aq) was added to the first solution in the reaction vessel under magnetic stirring and degassed an additional 5 min. Once degassed, 0.363 g of $NaBH_4$ was added and allowed to react for 20 min, followed by the addition of the Ni^{2+} micelle solution for 5 min. The purpose of the Ni^{2+} in this reaction is to aid in the formation of the iron oxide passivation layer for the iron core.[11] The reaction was then quenched by the addition of 100 mL of a 50/50 chloroform and methanol mixture. The precipitate was then washed with methanol several times while the Fe−Ox nanoparticles were collected via magnetic separation using a rare earth bar magnet with a 3 kOe field on the surface of the magnet.

2.3. Surface Functionalization. The preparation of the functionalized nanoparticles coated with dopamine (Fe−Ox dopamine) was performed by methods similar to those of Xu et al.,[9] but without preliminary functionalization of the terminal amine. Fe−Ox nanoparticles were sonicated for 45 min in cyclohexane or methanol with excess dopamine hydrochloride to ensure the maximum coating. The particles could then be extracted into water from the cyclohexane or magnetically separated from the methanol. The Fe−Ox dopamine particles with PEG functionalized to the dopamine through an amide bond (Fe−Ox dopamine/PEG) were prepared with the functionalization step being completed first, followed by sonication to bond the dopamine end of the ligand to the iron oxide shell. Functionalization was attempted on particles directly after synthesis, particles that were dried and exposed to air after synthesis, and under a N_2 atmosphere. None of the variations affected the initial Fe−Ox−dopamine complex, and thus functionalization was carried out in air for experiments due to simplicity.

2.4. Theoretical and Computational Methods. First principles theoretical studies were carried out to elucidate the electronic bonding of dopamine and its effect on the geometric and electronic structure of Fe_2O_3 particles. This understanding is critical for any applications of the system. The real nanoparticles contain several hundred to thousands of atoms, and first principles electronic structure studies on such large systems are computationally prohibitive. However, the insight into the microscopic mechanisms can be gained via studies on representative clusters chosen to depict the bonding pattern in the actual nanoparticle. Bulk α-Fe_2O_3 has a corundum structure and can be described as a hexagonal close-packed array of oxygen atoms in which two-thirds of the octahedral holes are occupied by the Fe atoms. The structure can also be viewed as the FeO_6 octahedron linked together by sharing edges, faces, or vertices. A small cluster that can represent the arrangement in the bulk structure and composition is a Fe_2O_3 cluster consisting of a distorted triangular bipyramid consisting of O atoms forming a triangle and with two Fe atoms occupying the apex sites. In such a structure, the oxygen sites are bonded to two Fe atoms, like the situation in bulk surfaces. However, as shown previously, the ground-state geometry of a free Fe_2O_3 cluster is a distorted Fe_2O_2 rhombus with an extra O attached to one of the Fe sites.[12] In this work, we therefore carried out investigations employing the triangular bipyramid as well as the open rhombus decorated structures. As we will show, the key conclusions are independent of the choice of the geometry.

The electronic structure investigations were carried out within a density functional formalism.[13] The exchange and correlation effects are included using the generalized gradient approximation (GGA) of Perdew, Burke, and Ernzerhof.[14] The electronic structure was obtained using a linear combination of atomic orbitals molecular orbital approach. Here, the wave function of the cluster is constructed through a linear combination of Gaussian-type orbitals centered at the atomic sites in the cluster. All calculations were performed using the deMon2K software.[15] Here, an auxiliary function set is used for the variational fitting of the Coulomb potential.[16,17] The numerical integration of the exchange-correlation energy and potential was performed on an adaptive grid.[18] The wave functions were formed using double-ζ valence polarized (DZVP) basis sets[19] for C, H, N, and O and the Wachters-F basis set[20−22] for Fe. The GEN-A2 auxiliary function set for C, H, N, and O and the GEN-A2* auxiliary function set for Fe were used. To determine the ground state, the configuration space was sampled by starting from several initial configurations and optimizing the geometry by moving atoms in the direction of forces till they dropped below a threshold value. Because transition metal atoms are marked by nonzero spin multiplicities, the ground-state determination included investigation over spin multiplicities. The geometries were optimized without any symmetry constraint using delocalized internal coordinates with the rational function optimization (RFO) and the Broyden, Fletcher, Goldfarb, and Shanno (BFGS) update.[23]

3. Results and Discussion

Attempts to use dopamine as a robust anchor on Fe−Ox were initially successful in dispersing the particles, forming a clear,

(11) Carpenter, E. E.; Calvin, S.; Stroud, R. M.; Harris, V. G. *Chem. Mater.* **2003**, *15*, 3245.
(12) Jones, N. O.; Reddy, B. V.; Rasouli, F.; Khanna, S. N. *Phys. Rev. B* **2005**, *72*.
(13) Kohn, R. W.; Sham, L. J. *Phys. Rev.* **1965**, *140*, A1133.
(14) Perdew, J. P.; Burke, K.; Ernzerhof, M. *Phys. Rev. Lett.* **1996**, *77*, 3865.
(15) Köster, A. M.; Calaminici, P.; Casida, M.; Flores-Moreno, R.; Geudtner, G.; Goursot, A.; Heine, T.; Ipatov, A.; Janetzko, F.; Patchkovskii, S.; Reveles, J. U.; Vela, A.; Salahub, D. R. *The International deMon Developers Community*; deMon2k V.1.8, 2005; http://www.deMon-software.com.
(16) Mintmire, J. W.; Dunlap, B. I. *Phys. Rev. A* **1982**, *25*, 88.
(17) Dunlap, B. I.; Connolly, J. W. D.; Sabin, J. R. *J. Chem. Phys.* **1979**, *71*, 4993.
(18) Köster, A. M.; Flores-Moreno, R.; Reveles, J. U. *J. Chem. Phys.* **2004**, *121*, 681.
(19) Godbout, N.; Salahub, D. R.; Andzelm, J.; Wimmer, E. *Can. J. Chem.* **1992**, *70*, 560.
(20) Bauschlicher, C. W., Jr.; Langhoff, S. R.; Barnes, L. A. *J. Chem. Phys.* **1989**, *91*, 2399.
(21) Wachters, A. J. H. *IBM Tech. Rep.* **1969**, RJ584.
(22) Wachters, A. J. H. *J. Chem. Phys.* **1970**, *52*, 1033.
(23) Reveles, J. U.; Köster, A. M. *J. Comput. Chem.* **2004**, *25*, 1109.

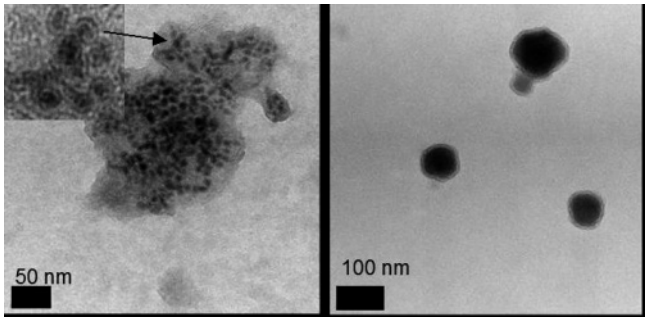

Figure 1. The first TEM (left) is Fe/iron oxide core−shell particles coated with dopamine (Fe−Ox dopamine) and immediately dried on the TEM grid. The other TEM (right) is of the precipitated particles after 1 day in aqueous solution. Inset on the left image is a zoomed region for better viewing of the core−shell concentric rings. Note that the particles have changed in size dramatically.

blue/purple aqueous ferrofluid. After remaining in solution for 1 day, however, the particles turned to a dark green precipitate. This precipitate is a combination of both precipitated iron oxide particles (black-magnetite/maghemite) and iron(II) hydroxide (green). Upon further oxidation, the green color turned to a red/brown, which is typical of iron(III) oxyhydroxide.[24] The transmission electron micrograph presented in Figure 1 (left) contains functionalized nanoparticles that were immediately dried after sonication. This micrograph shows that the particles are spherical and also reveals the presence of concentric rings and a "cloudy" region around the particles. The observed aggregation is a result of the evaporative sample grid preparation. The rings around the particles are due to changes in electron density between the iron core and iron oxide shells. The granular substrate can be seen clearly, and the rings are present when over or under focus, thus eliminating the possibility that these features are just imaging artifacts. The "cloudy" region can be attributed to the electron density being donated to the surrounding dopamine from the Fe−Ox particles and the presence of ferric catechol hydrogen bound to the dopamine layer. To help elucidate the absorbed dopamine's reactivity and structure, we employed several experimental techniques as well as total energy calculations using first principles theoretical studies. Figure 1 (right) is a micrograph of the precipitate after a solution of Fe−Ox dopamine particles was aged for 1−2 days. More importantly, the differences seen in the TEM images in Figure 1 illustrate that the nanomorphology of the particles is lost, thus implying a surface reaction between the Fe^{3+} in the iron oxide shell and dopamine instead of the formation of two "robust" Fe−O bonds.[9]

Further evidence of a surface reaction can be seen in the mid-IR in Figure 2. The spectrum of dopamine exhibits a clear and broad OH stretch centered around 3300 cm^{-1}. The spectrum of the plain Fe−Ox particles also contains an OH stretch due to surface absorbed water that through intermolecular bonding forms an iron hydroxide hydration shell. The center of this absorbance is shifted to around 3400 cm^{-1} due to a higher degree of intermolecular bonding at the surface of the nanoparticles. The center of the OH absorbance of Fe−Ox dopamine shifts to even higher energy at 3500 cm^{-1}, which is typical for an alcohol or phenol stretch that is intermolecular bonded.[25] This absorbance band also seems to have more than one maximum in the range from 3600 to 3400 cm^{-1}, which is due to differing proton location, such as being coordinated between the catechol oxygens, between a catechol oxygen and surface oxide, or just an OH of the surface hydroxide. These different proton arrangements can also be described as the intermediate between the dopamine semiquinone complex (compound **2**) and the dopamine quinone complex (compound **3**), or possibly to protons coordinated to the oxygen in the initial Fe−Ox dopamine complex (compound **1**). The IR spectrum of Fe−Ox dopamine also contains a peak at 1650 cm^{-1} that extends through a broad hump to 1590 cm^{-1}, which is indicative of an aromatic ketone and the enol of a diketone. [25] This can be attributed to the equilibrium between compounds **2** and **3**. El-Ayaan et al. also show that if compound **3** is in an acidic environment, there is a ring closure through an internal Michael addition to form leucodopaminochrome (compound **4**), and then with more Fe^{3+} there is conversion to dopaminochrome.[26]

To further investigate the steps in the reaction, UV−vis spectra of dopamine and a solution of Fe−Ox dopamine particles were analyzed at three points in time. As expected, there is a difference in the absorbance data of dopamine as compared to the Fe−Ox dopamine particles. Absorptions were seen for the Fe−Ox dopamine particles between 210 and 300 nm, which are due to the charge-transfer (CT) bands of $Fe^{3+/2+}$ complexes.[27,28] The fact that peaks in this region are also present for $\pi \rightarrow \pi^*$ transitions in dopamine, and remain in the supernate after all of the particles have precipitated out of solution, makes it hard to draw many conclusions about the reaction taking place. On the other hand, a broad absorbance band was noted around 584 nm, which is related to the d−d transitions of $Fe^{3+/2+}$. The reduction in intensity of this band after 24 h is clear evidence of less $Fe^{3+/2+}$ in solution. Once the concentration of $Fe^{3+/2+}$ is too low, the d−d bands are no longer visible because they are overwhelmed by the intensity of the CT bands; thus more iron must have precipitated out.

If the reaction went through the full oxidation process to form dopaminochrome, we would expect to observe a strong absorbance band around 400 nm, which is indicative of a quinone. On the other hand, the absence of this band is expected for leucodopaminochrome (compound **4**) because it is UV-transparent. The ring closure of the quinone to form compound **4** is spontaneous with a high reaction rate constant[26] and reacts faster when exposed to light, thus making it difficult to ensure that the degradation of the particles is oxidizing the dopamine through the quinone state. To capture this portion of the reaction, dopamine was first functionalized with PEG before reacting with the Fe−Ox particles to prevent the ring closure from occurring. The UV−vis spectrum of the Fe−Ox dopamine/PEG particles in Figure 3 revealed an absorbance around 420 nm, which is typical for the quinone of dopamine,[10] thus providing evidence for the formation of the quinone in this reaction mechanism.

(24) Cornell, R. M.; Schwertmann, U. *The Iron Oxides: Structure, Properties, Reactions, Occurence and Uses*; VCH: New York, 1996.

(25) Silverstein, R. M.; Webster, F. X.; Kiemle, D. J. *Spectrometric Identification of Organic Compounds*; John Wiley & Sons: New York, 2005; Vol. 7, p 119.

(26) ElAyaan, U.; Herlinger, E.; Jameson, R. F.; Linert, W. *J. Chem. Soc., Dalton Trans.* **1997**, *16*, 2813−2818.

(27) Bordiga, S.; Buzzoni, R.; Geobaldo, F.; Lamberti, C.; Giamello, E.; Zecchina, A.; Leofanti, G.; Petrini, G.; Tozzola, G.; Vlaic, G. *J. Catal.* **1996**, *158*, 486−501.

(28) Umamaheswari, V.; Bohlmann, W.; Poppl, A.; Vinu, A.; Hartmann, M. *Microporous Mesoporous Mater.* **2006**, *89*, 47−57.

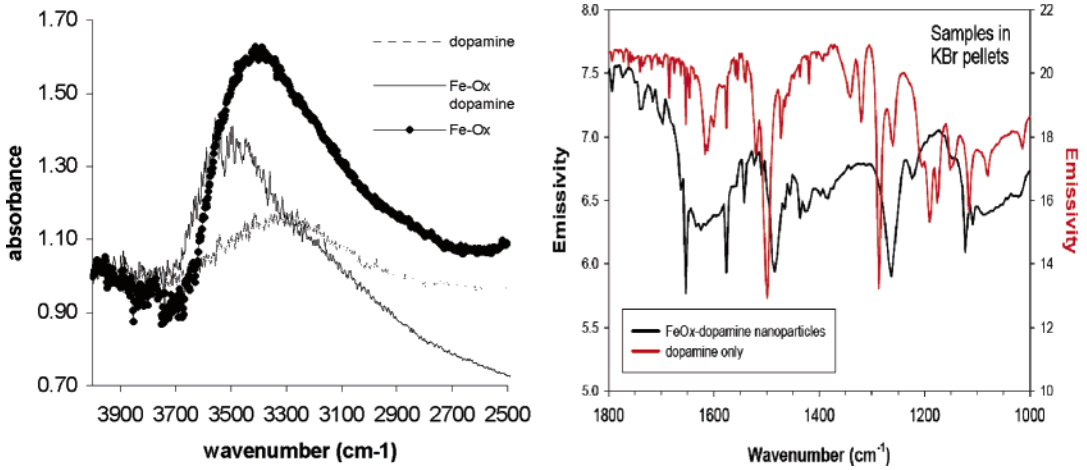

Figure 2. (Left) Mid-IR spectra from 4000 to 2390 cm^{-1} of Fe/iron oxide core−shell particles (Fe−Ox), dried Fe−Ox dopamine particles, and dopamine hydrochloride (dopamine). These samples were prepared in AgBr pellets to minimize water interference in this region because AgBr is less hygroscopic than KBr. (Right) Mid-IR spectra from 1800 to 1000 cm^{-1} of Fe/iron oxide core−shell particles coated with dopamine (Fe−Ox dopamine) and dopamine hydrochloride prepared in KBr pellets.

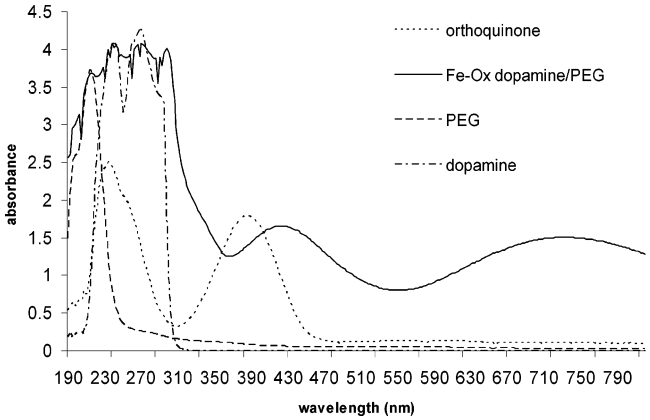

Figure 3. UV−vis spectra of orthoquinone, Fe−Ox dopamine/PEG, PEG, and dopamine showing the contribution of each component to the overall spectrum of Fe−Ox dopamine.

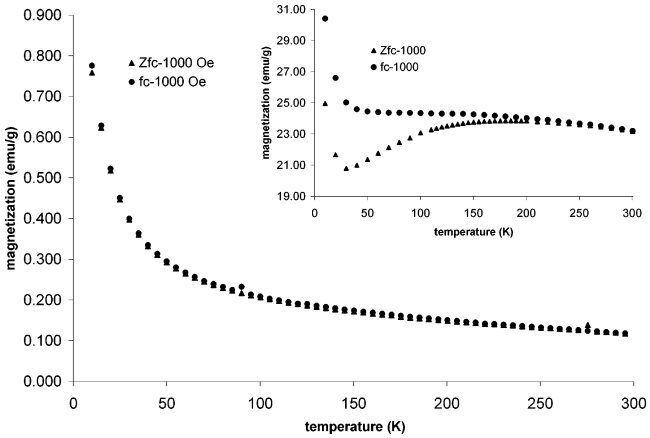

Figure 4. Magnetization versus temperature plots at an applied field of 1000 Oe for Fe−Ox dopamine particles (inset) and for the precipitate material after 1−2 days.

Magnetic characterization was carried out on both the initially dried Fe−Ox dopamine particles and the aged precipitate to further investigate changes in the material due to this Fe^{3+}−dopamine reaction. A magnetization versus temperature plot at 1000 Oe, seen in the inset of Figure 4, demonstrates that the Fe−Ox dopamine particles exhibit superparamagnetic behavior with a paramagnetic tail at low temperatures due to the dopamine. A hysteresis plot yielded a saturation magnetization of 80 emu/g at 10 K, which is fairly high because we included the mass of dopamine in this calculation. The precipitate material revealed predominantly paramagnetic behavior as seen in Figure 4, but also showed slight ferromagnetic behavior in a hysteresis plot, which could be due to small iron oxide particles surrounded by large amounts of iron oxyhydroxide. Elemental analysis by ICP-OES revealed that the dark precipitate was 24.2% Fe, thus ensuring the presence of Fe in the material. To determine what the oxidation state of the iron was, a Curie−Weiss fit was performed on the data, suggesting Fe^{3+}, most likely in the oxyhydroxide form that would be red/brown in color and often forms when $Fe(OH)_2$ (green) oxidizes in water. The fit revealed deviation from Curie−Weiss law at higher temperatures, which is most likely due to enhanced coupling between the small amounts of magnetite that remain. A linear fit to the lower temperature portion and using the Lande constant for iron gave a total spin of $^5/_2$, which would be expected for Fe^{3+}.

Now that our experimental data have put together pieces that support the decomposition of the nanoparticles and dopamine, we will look at the modeling of a comparative system to give further insight into the mechanism. The key issue, answered by the first principles calculations, is how the dopamine is absorbed on a Fe_2O_3 surface, or is it just a surface reaction that leads to the degradation of the Fe−Ox nanoparticles? The later possibility would exist if the heat of adsorption is sufficient to break a cluster into two fragments. For each cluster X_nY_m involved in such a process, we first determined the atomization energy, AE, defined by

$$\mathrm{AE} = nE(\mathrm{X}) + mE(\mathrm{Y}) - E(\mathrm{X}_n\mathrm{Y}_m)$$

Here, $E(X_nY_m)$ is the total energy of the cluster, while $E(X)$ and $E(Y)$ are the total energies of the individual atoms. With such a definition, positive values of AE represent the energy required to break the cluster into isolated atoms. Using the calculated AE, we investigated the energetics of the process involving attachment of semiquinone ($C_8H_{10}NO_2$) to a Fe_2O_3 cluster and breaking of the complex into various possible

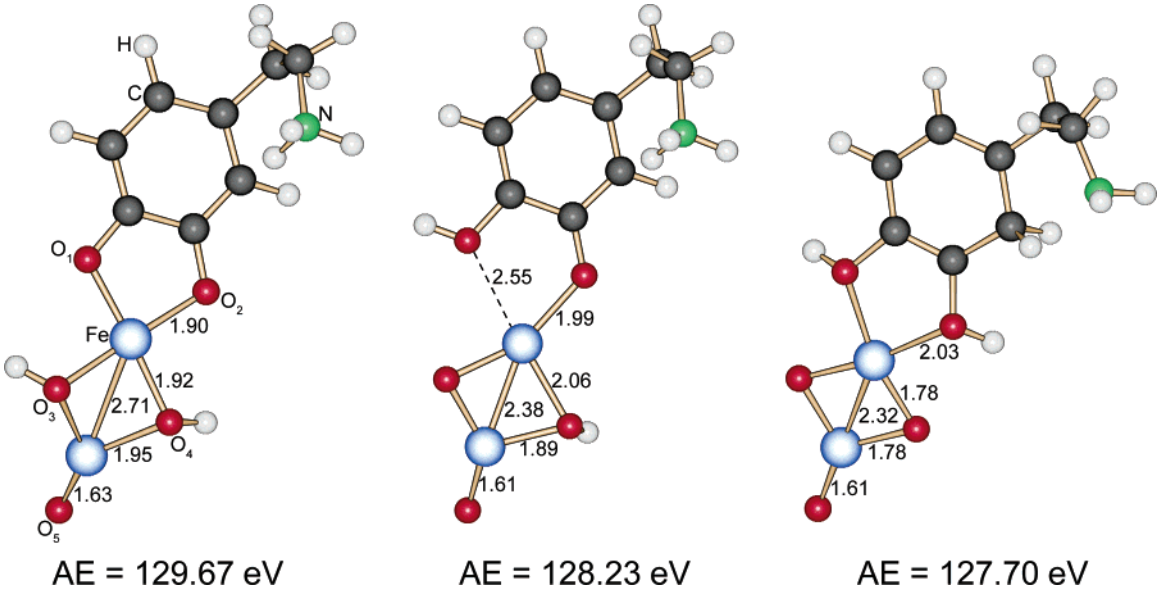

Figure 5. Structural geometries and resulting AE's for different protonation sites for the Fe_2O_3 and dopamine semiquinone complex. Bond lengths are in angstroms.

products. We first consider the attachment energy according to the reaction:

$$^2\text{semiquinone} + {}^3Fe_2O_3 \rightarrow {}^2Fe_2O_3\text{–semiquinone} \qquad \Delta E = 3.29 \text{ eV} \quad (1)$$

Here, the superscripts represent the ground-state spin multiplicity, and the positive sign in ΔE indicates that the reaction is exothermic. Next, two possible fragmentation reactions were explored, and in the following we provide the energetics for each of the processes:

$$^2Fe_2O_3\text{–semiquinone} \rightarrow {}^4\text{FeO}-\text{semiquinone} + {}^3FeO_2 \qquad \Delta E = -3.67 \text{ eV} \quad (2)$$

$$^2Fe_2O_3\text{–semiquinone} \rightarrow {}^6\text{Fe}-\text{semiquinone} + {}^1FeO_3 \qquad \Delta E = -4.99 \text{ eV} \quad (3)$$

As we notice, reaction 2 requires 3.67 eV of energy, while reaction 3 requires 4.99 eV of energy to proceed. This would seem to imply that the semiquinone can bind to Fe_2O_3 without degradation of the parent cluster.

While this is encouraging, the actual solution contains H^+ cations, and one has to ascertain the stability in the presence of these protons. As a first example, we consider the case when two protons bind to the cluster. Here, we started with a Fe_2O_3–semiquinone cluster and first investigated where the two protons would prefer to bind. For example, the protons could bind to O sites closer to the semiquinone, or prefer to bind to O sites farther from semiquinone. These possibilities along with the resulting AE are given in Figure 5. Note that the more stable situation corresponds to proton binding to oxygens labeled O_3 and O_4. The preference of the proton to these oxygens can be explained by differences in electronegativity. The oxygens O_1 and O_2 are bridged between an iron and the delocalized negative charge of the benzene ring. This would cause the oxygens

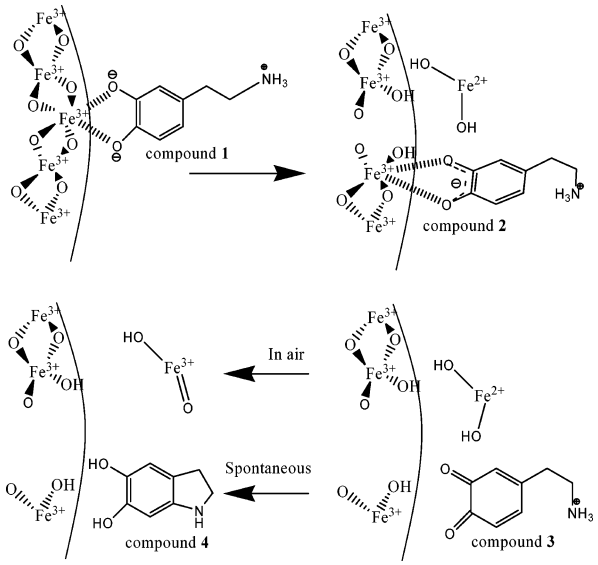

Figure 6. Proposed mechanism for the decomposition of Fe_2O_3 nanoparticles by dopamine in an aqueous solution. (Top left) Illustration of the initial complex formed in the coordination of dopamine on the surface of the nanoparticle. (Top right) Formation of the semiquinone complex through the first electron transfer and iron(II) hydroxide fragmentation. (Bottom right) Second electron transfer to form the dopamine quinone and second fragmentation. (Bottom left) Michael addition that forms the UV transparent leucodopaminochrome and the oxidation of $Fe(OH)_2$ that forms the FeOOH.

bridged between two irons to be more electronegative, thus also making O_3 and O_4 electrostatically favored for proton binding. Also, in the case of the protonation O_1 and O_2, only one O–Fe bond is broken or the two O–Fe bonds are just stretched from 1.91 (nonprotonated) to 2.03 Å (Figure 5). Having found this, we now investigated the energetics of the process where a Fe_2O_3 with H atoms ligated at the oxygens O_3 and O_4 approaches the semiquinone and whether the heat of formation is enough to drive the cluster to cleavage. The attachment energy is given by the equation:

$$^2\text{semiquinone} + {}^7Fe_2O_3H_2 \rightarrow {}^6Fe_2O_3H_2\text{–semiquinone} \qquad \Delta E = 3.47 \text{ eV} \quad (4)$$

(29) Grillo, V. A.; Hanson, G. R.; Wang, D. M.; Hambley, T. W.; Gahan, L. R.; Murray, K. S.; Moubaraki, B.; Hawkins, C. J. *Inorg. Chem.* **1996**, *35*, 3568–3576.

In the following, we outline the results of the fragmentation reaction involving breaking of the complex with two hydrogens attached to O_3 and O_4.

$$^{6}Fe_2O_3H_{2-}\text{semiquinone} \rightarrow {}^{6}\text{Fe}-\text{semiquinone} + {}^{5}FeO_3H_2 \qquad \Delta E = -3.28\ \text{eV} \quad (5)$$

As seen from eq 5, the attachment of the semiquinone does lead to a decrease on the fragmentation energy as compared to the intact structure in the absence of H atoms (eq 3). We found that (not shown here) addition of 4 H atoms leads to even easier breaking of the Fe_2O_3.

We then calculate the energy required to fragment the bare and hydrogenated Fe_2O_3 cluster in the presence of the semiquinone according to the reactions:

$$^{2}\text{semiquinone} + {}^{3}Fe_2O_3 \rightarrow {}^{6}\text{Fe}-\text{semiquinone} + {}^{1}FeO_3 \qquad \Delta E = -1.70\ \text{eV} \quad (6)$$

$$^{2}\text{semiquinone} + {}^{7}Fe_2O_3H_2 \rightarrow {}^{6}\text{Fe}-\text{semiquinone} + {}^{5}FeO_3H_2 \qquad \Delta E = 0.19\ \text{eV} \quad (7)$$

According to eq 5, the reaction is exothermic and the hydrogenated Fe_2O_3 cluster will be fragmented.

The mechanism and reaction rates of the oxidation of catechols by ferric cations have been proposed,[26,29] but now we outline the mechanism for the decomposition of nanoparticles functionalized by dopamine (Figure 6). Following the initial proposed mechanism, the reaction initially forms an iron(III) complex (compound **1**) on the surface of the nanoparticle. Formation of the initial structure with the dopamine coordinated to the surface of the iron oxide nanoparticle is a result of improved orbital overlap of the five-membered ring as well as the reduced steric environment of the iron complex. This five-membered ring leads to a far more stable structure than the typical four-membered metallocycle seen with carboxylic acid complexes. Through the transfer of one electron, the dopamine is oxidized to form a semiquinone (compound **2**), but the complex is still coordinated to the surface of the nanoparticle. As shown in our calculations, the free protons in the solution more favorably coordinate with the inner oxygens connected to the Fe^{2+}. This reduces the overall energy of the system and then allows the dopamine to shift to other Fe^{3+} on the surface, and the Fe^{2+} then is free to be released into the solution as a hydroxide, which in air will oxidize to FeOOH. The semiquinone compound re-forms on adjacent Fe^{3+} on the surface. With one more electron transfer, the semiquinone is then converted into an orthoquinone (compound **3**). The orthoquinone then spontaneously converts to compound **4**, and the resultant functionalized nanoparticle is now less stable.

All of the reported results demonstrate that the reactivity between Fe^{3+} and dopamine quickly facilitates the degradation of the nanoparticles. The degradation process can only be slowed slightly by the addition of a large ligand through the terminal amine, but is also detrimental because a greater presence of the dopamine quinone can be cytotoxic. The energetic modeling studies also substantiate our proposed decomposition mechanism and thus conclude that the use of dopamine as a robust anchor for iron oxide or iron oxide shell particles will not fulfill the need for stable dispersions for use in most biomedical applications.

Acknowledgment. J.U.R. acknowledges support from the U.S. Air Force Office of Scientific Research grant FA9550-05-1-0186, while S.N.K. is grateful to the U.S. Department of Energy for support from grant DE-FG02-96ER45579. S.N.K. is also grateful to VCU for a study/research leave. E.E.C. would like to thank the Thomas and Kate Jeffress Memorial Trust grant J-815 and the PM-USA INEST group for financial support.

Supporting Information Available: Additional spectroscopic, magnetic, and theoretical data. This material is available free of charge via the Internet at http://pubs.acs.org.

JA0651963